MATERIALE PLASTICE
https://revmaterialeplastice.ro
https://doi.org/10.37358/Mat.Plast.1964

A Hydrogel-Based *In Vitro* Coculture Model for Studying Aging-Associated Granulosa Cell–Endothelial Cell Interaction

QIANQIAN MA[1,#*], HAN ZHENG[2,#], AILING CHEN[3,#], JINGFEN CAI[4], LIFENG ZHANG[5*], YANFANG GU[4*]

[1] Department of Maternity and Child Health Care, Wuxi Maternity and Child Health Care Hospital, Women's Hospital of Jiangnan University, Wuxi, China
[2] Department of Public Health, Wuxi Maternity and Child Health Care Hospital, Women's Hospital of Jiangnan University, Wuxi, China
[3] Department of Obstetrics and Gynecology, Wuxi Maternity and Child Health Care Hospital, Women's Hospital of Jiangnan University, Wuxi, China
[4] Department of Gynecology, Wuxi Maternity and Child Health Care Hospital, Women's Hospital of Jiangnan University, Wuxi, China
[5] Department of Obstetrics and Gynecology, Taicang Traditional Chinese Medicine Hospital, Taicang, China

Abstract: ***Background:*** *A suitable biomaterial scaffold is essential for building in vitro ovarian models. This study developed a GelMA/HAMA (GH) hydrogel to support granulosa cell culture and to construct a simplified coculture system for granulosa cell–endothelial cell interaction.* ***Methods:*** *GH hydrogel was characterized by rheology, tensile testing, scanning electron microscopy, swelling, degradation, and extract-based cytocompatibility. KGN granulosa cells were encapsulated in GH hydrogel, and an aging-like model was induced with H_2O_2. A Transwell system and conditioned-medium experiments were used to evaluate endothelial cell responses.* ***Results:*** *GH hydrogel showed light-triggered gelation, predominantly elastic behavior, higher tensile performance than GelMA, lower swelling, and slower degradation, with acceptable cytocompatibility at the tested range. In KGN-laden hydrogels, H_2O_2 treatment increased ROS and p16 expression while decreasing E2 secretion and StAR expression. Conditioned medium from aging granulosa cells increased ROS and VCAM-1 and reduced HUVEC viability.* ***Conclusion:*** *GH hydrogel provides a controllable matrix for granulosa cell culture and a useful in vitro platform for studying aging-related granulosa cell–endothelial cell crosstalk.*

Keywords: *GelMA/HAMA hydrogel, granulosa cells, ovarian aging, endothelial cells, coculture model*

1. Introduction

In vitro ovarian models require not only appropriate cell sources but also suitable material platforms capable of providing a permissive microenvironment for cell survival, phenotype maintenance, and intercellular communication [1]. Conventional two-dimensional culture systems are easy to operate, but they cannot adequately reproduce the hydrated, spatially organized, and matrix-dependent environment surrounding ovarian cells [2,3]. For granulosa cells in particular, cell behavior is closely influenced by extracellular matrix support and by soluble factor exchange with neighboring cell populations [4]. Therefore, the selection of a biomaterial scaffold is a key consideration when establishing an *in vitro* model intended to study ovarian-related cellular responses [5–7].

Hydrogels are widely used in tissue-related *in vitro* models because of their high water content, soft nature, and structural similarity to native extracellular matrices. Among them, gelatin methacrylate (GelMA) has attracted considerable attention due to its good biocompatibility, photocrosslinkability, and the presence of cell-interactive motifs derived from gelatin [8]. However, GelMA-only systems may not always provide optimal hydration behavior, structural stability, or matrix composition for specific

*email: 9862023234@jiangnan.edu.cn; zhangzhang110521@163.com; gyf21035378@163.com
[#] *These authors contributed equally to this work*

cell models [9]. Hyaluronic acid is an important component of the native extracellular environment in many tissues, and its methacrylated derivative, HAMA, offers the possibility of introducing additional hydrophilicity and matrix-related biochemical characteristics into photocurable hydrogel systems [10]. In this context, combining GelMA with HAMA represents a practical material strategy for constructing a more suitable three-dimensional culture matrix. In the present work, GelMA and HAMA were combined with LAP photoinitiator to prepare a photocrosslinkable GH hydrogel, which was subsequently used as the matrix for granulosa cell encapsulation [11].

From a materials perspective, a hydrogel intended for cell-laden culture should meet several basic requirements [12]. First, it should undergo reliable gelation under mild conditions to enable convenient encapsulation and shaping. Second, it should possess appropriate viscoelastic and mechanical properties to maintain structural integrity during culture. Third, its swelling and degradation behavior should be sufficiently controlled to avoid excessive instability while still preserving a hydrated environment. Finally, the material should exhibit acceptable cytocompatibility under the intended experimental conditions [13]. In this study, the GH hydrogel was designed and characterized from these aspects, including gelation behavior, rheological response, tensile properties, internal morphology, swelling, enzymatic degradation, and extract-based cytocompatibility. These evaluations were necessary to determine whether the material was suitable for subsequent biological experiments.

Based on this material platform, granulosa cells were encapsulated in GH hydrogel to establish a three-dimensional ovarian-side model, and a Transwell system was further introduced to investigate indirect communication between granulosa cells and endothelial cells through soluble factors. This design did not aim to fully reconstruct the complexity of native ovarian tissue, but rather to provide a controllable material-based *in vitro* system in which the influence of granulosa cell status on endothelial cell responses could be examined under defined conditions. Accordingly, the purpose of this study was to develop and characterize a GelMA/HAMA hydrogel platform for granulosa cell culture and to explore its applicability in a simplified coculture model related to ovarian aging-associated microenvironmental changes. The novelty of this study lies not simply in the use of GelMA, HAMA, or a Transwell system individually, but in integrating a GelMA/HAMA hydrogel matrix with an aging-like granulosa cell model and an endothelial cell response system. This design provides a simplified and controllable *in vitro* platform for investigating soluble-factor-mediated communication between aging-like granulosa cells and endothelial cells. Compared with conventional two-dimensional granulosa cell culture, the present model provides a three-dimensional hydrogel microenvironment for granulosa cells. Compared with more complex ovarian follicle or vascular niche models, this system is intentionally simplified to focus on paracrine granulosa cell-endothelial cell interaction under defined experimental conditions.

2. Materials and methods

2.1. Materials

Gelatin methacrylate (GelMA), methacrylated hyaluronic acid (HAMA), and lithium phenyl-2,4,6-trimethylbenzoylphosphinate (LAP) were purchased from Aladdin (Shanghai, China). Dulbecco's modified Eagle's medium/Ham's F-12 (DMEM/F12), fetal bovine serum (FBS), penicillin–streptomycin, phosphate-buffered saline (PBS), trypsin–EDTA, endothelial cell medium, Cell Counting Kit-8 (CCK-8), type I collagenase, hydrogen peroxide (H_2O_2), and 2′,7′-dichlorodihydrofluorescein diacetate (DCFH-DA) were purchased from Beyotime Biotechnology (Shanghai, China) or Gibco (Grand Island, NY, USA). Human granulosa-like KGN cells were obtained from Procell (Wuhan, China). Human umbilical vein endothelial cells (HUVECs) were obtained from ScienCell (Carlsbad, CA, USA). The estradiol (E2) ELISA kit was purchased from Elabscience (Wuhan, China). TRIzol reagent, reverse transcription kit, and SYBR Green qPCR master mix were purchased from Vazyme (Nanjing, China).

2.2. Cell culture

KGN cells were cultured in DMEM/F12 supplemented with 10% FBS and 1% penicillin–streptomycin at 37°C in a humidified incubator containing 5% CO_2. HUVECs were cultured in endothelial cell medium supplemented with 5% FBS, 1% endothelial cell growth supplement, and 1% penicillin–streptomycin under the same conditions. The culture medium was changed every 2 days, and cells at passages 3–6 were used for experiments.

2.3. Preparation of GelMA, HAMA, and GH hydrogel

GelMA and HAMA were dissolved in sterile PBS containing LAP under light-protected conditions at 37°C until fully dissolved. The final concentration of the GH precursor solution was 10% (w/v) GelMA, 1% (w/v) HAMA, and 0.25% (w/v) LAP. Pure GelMA precursor was prepared at 10% (w/v) GelMA with 0.25% (w/v) LAP and used as the control hydrogel where indicated. The precursor solutions were sterilized by filtration through a 0.22 μm filter. For gel formation, the precursor was transferred into the required mold or culture insert and exposed to 405 nm light at 10 mW/cm^2 for 30 s.

2.4. Rheological characterization

Rheological measurements were performed using a rotational rheometer (MCR 302, Anton Paar, Austria) equipped with a 25 mm parallel-plate geometry. Frequency sweep tests were conducted at 25°C over an angular frequency range of 0.1–100 rad/s at 1% strain, which was within the linear viscoelastic region. The storage modulus (G') and loss modulus (G'') of GelMA and HAMA were recorded.

For time sweep measurements of GH hydrogel, the precursor solution was loaded directly onto the rheometer plate and measured at a constant angular frequency of 1 rad/s and a strain of 1%. After an initial baseline period, gelation was triggered by 405 nm light irradiation, and the changes in G' and G'' were monitored continuously for 300 s.

2.5. Tensile mechanical testing

Hydrogel samples were cast into dumbbell-shaped silicone molds with a gauge length of 10 mm, width of 4 mm, and thickness of 2 mm, followed by photo-crosslinking under the same conditions described above. Tensile tests were performed using a universal testing machine (Instron 3343, Instron, USA) equipped with a 100 N load cell. The crosshead speed was set at 10 mm/min. Engineering stress was calculated by dividing the tensile force by the initial cross-sectional area, and engineering strain was calculated from the ratio of extension to initial gauge length. Representative stress–strain curves were used for comparison.

2.6. Scanning electron microscopy

For SEM observation, GH hydrogel samples were first frozen at −80°C and then lyophilized for 48 h. The dried samples were fractured to expose the internal cross-section and sputter-coated with gold for 60 s using a sputter coater (SC7620, Quorum Technologies, UK). The samples were observed with a scanning electron microscope (SU8010, Hitachi, Japan) at an accelerating voltage of 5 kV.

2.7. Swelling assay

Hydrogel samples with identical dimensions were prepared and weighed immediately after gelation to obtain the initial mass. Samples were then immersed in PBS at 37°C. At predetermined time points (0, 2, 5, 8, 12, 16, 20, 24, 30, 36, 42, and 48 h), the samples were removed, gently blotted with filter paper to remove excess surface water, and weighed to obtain swelling ratio. The swelling ratio was calculated using the following equation:

$$\text{Swelling ratio}\,(\%) = (\text{Wt} - \text{W0})\,/\text{W0} \times 100\%$$

where W0 represents the initial mass of the hydrogel immediately after gelation, and Wt represents the mass of the swollen hydrogel at each time point.

2.8. Enzymatic degradation assay

GelMA and GH hydrogel samples of the same size and initial mass were incubated in PBS containing 1 mg/mL type I collagenase at 37°C. At days 0, 1, 2, 3, 4, 5, 6, and 7, samples were collected, washed briefly with PBS, gently blotted to remove excess liquid, and weighed. The remaining mass percentage was calculated using the following equation:

$$\text{Remaining mass } (\%) = \text{Wt/W0} \times 100\%$$

where W0 represents the initial mass of the hydrogel before degradation, and Wt represents the remaining mass of the hydrogel at each degradation time point.

2.9. Extract-based cytocompatibility assay

Sterile GH hydrogel was incubated in serum-free culture medium at extraction concentrations of 0.1 and 0.2 g/mL at 37°C for 24 h to obtain hydrogel extracts. Cells were seeded into 96-well plates at a density of 5×10^3 cells/well and cultured overnight. The medium was then replaced with blank control medium or the corresponding extract-containing medium. After 24 h incubation, 10 μL CCK-8 reagent was added to each well containing 100 μL medium and incubated for 2 h at 37°C. Absorbance at 450 nm was measured using a microplate reader (Synergy H1, BioTek, USA). Cell viability was normalized to the blank control group.

2.10. Construction of the granulosa cell-laden GH hydrogel model

KGN cells were suspended in GH precursor solution at a final density of 1×10^6 cells/mL. The cell-containing precursor was transferred into culture inserts or molds and crosslinked under 405 nm light to form a granulosa cell-laden GH hydrogel model. For basic phenotype evaluation, the cell-laden hydrogels were maintained in complete DMEM/F12 medium under standard culture conditions.

2.11. Establishment of the aging granulosa cell model

To induce an aging-like state, KGN-laden GH hydrogels were treated with 200 μM H_2O_2 for 24 h. The control group was cultured in fresh medium without H_2O_2. After treatment, the samples were washed twice with PBS and immediately used for downstream assays, including ROS measurement, E2 determination, and gene expression analysis.

2.12. Intracellular ROS assay

Intracellular ROS levels in KGN cells and HUVECs were measured using DCFH-DA. Briefly, cells were incubated with 10 μM DCFH-DA in serum-free medium at 37°C for 30 min in the dark, followed by washing three times with PBS. Fluorescence images were collected under a fluorescence microscope (IX73, Olympus, Japan), and the fluorescence intensity was quantified using ImageJ software. Relative ROS levels were normalized to the corresponding control group.

2.13. E2 secretion assay

To evaluate granulosa cell function, culture supernatants were collected from the control and aging KGN-laden GH hydrogel groups after 24 h incubation in fresh medium. The collected supernatants were centrifuged at 1000× g for 5 min to remove debris. E2 levels were then measured using a commercial ELISA kit according to the manufacturer's instructions. Absorbance was measured with a microplate reader, and E2 concentrations were calculated based on a standard curve.

2.14. Quantitative real-time PCR

Total RNA was extracted from KGN-laden GH hydrogels or HUVECs using TRIzol reagent. Complementary DNA was synthesized from 1 μg RNA using a reverse transcription kit. Quantitative real-time PCR was performed using SYBR Green Master Mix on a QuantStudio 5 Real-Time PCR

System (Applied Biosystems, USA). Relative expression levels were normalized to GAPDH and calculated using the $2^{-\Delta\Delta Ct}$ method.

The primer sequences were as follows:
StAR forward: 5′-TGGAGAGGCTTTCAAGGAGA-3′
StAR reverse: 5′-CCACACCTTGATGACCTTCC-3′
p16 forward: 5′-CGGCTGACTGGCTGGC-3′
p16 reverse: 5′-GGTCGGCGCAGTTGGGCTCC-3′
VCAM-1 forward: 5′-CAGGCTGTAAAAGAATTTGGAAAA-3′
VCAM-1 reverse: 5′-AAAGTGGTATTCAGGGGAAGTGTT-3′
AMH forward: 5′-CTGCTGCTGCTGCTACTTCT-3′
AMH reverse: 5′-GGGTCTTCCATGTTGATGGT-3′
GAPDH forward: 5′-GGAGCGAGATCCCTCCAAAAT-3′
GAPDH reverse: 5′-GGCTGTTGTCATACTTCTCATGG-3′

2.15. Transwell coculture system

A 12-well Transwell system with 0.4 μm pore-size inserts (Corning, USA) was used. HUVECs were seeded into the lower chamber at a density of 1×10^5 cells/well and allowed to attach overnight. KGN-laden GH hydrogels were placed in the upper Transwell inserts to form the ovarian-side compartment. The control and aging granulosa cell models were cultured in the upper insert, while HUVECs in the lower chamber served as the responder cells. The coculture system was maintained for 24 h under standard culture conditions. This setup allowed soluble factors to diffuse across the membrane while preventing direct cell–cell contact.

2.16. Preparation of conditioned medium

For conditioned medium experiments, control and aging KGN-laden GH hydrogels were washed with PBS and then incubated in fresh DMEM/F12 containing 1% FBS for 24 h. The collected supernatants were centrifuged at 1000× *g* for 5 min to remove suspended cells and debris. These supernatants were defined as normal conditioned medium (Normal CM) and aging conditioned medium (Aging CM), respectively.

2.17. Endothelial cell response assay

HUVECs were treated with blank medium, Normal CM, or Aging CM for 24 h. After treatment, intracellular ROS was measured using 10 μM DCFH-DA. VCAM-1 expression was analyzed by quantitative real-time PCR. Cell viability was assessed by CCK-8 assay. For the CCK-8 assay, HUVECs were seeded into 96-well plates at a density of 5×10^3 cells/well, treated with the indicated media for 24 h, followed by incubation with 10 μL CCK-8 reagent in 100 μL medium for 2 h at 37°C. Absorbance was measured at 450 nm.

2.18. Statistical analysis

All quantitative data were obtained from at least three independent experiments and are presented as mean ± standard deviation (SD). Statistical analyses were performed using GraphPad Prism 9.0 (GraphPad Software, USA). Comparisons between two groups were performed using an unpaired Student's *t* test. Comparisons among three or more groups were analyzed by one-way analysis of variance (ANOVA) followed by Tukey's post hoc test. A value of $p < 0.05$ was considered statistically significant.

3. Results

Figure 1 illustrates the overall design of the *in vitro* coculture system used in this study. Granulosa cells were first encapsulated in GelMA/HAMA hydrogel to establish the ovarian-side model. Based on different treatment conditions, normal and aging granulosa cell groups were generated in the upper

Transwell compartment. Endothelial cells were cultured in the lower chamber as the vascular-side responder cells. This configuration enabled the two cell types to remain spatially separated while allowing the exchange of soluble factors through the Transwell membrane. Therefore, the system was designed to simulate paracrine communication between granulosa cells and endothelial cells under controlled *in vitro* conditions. On this basis, the effects of normal or aging granulosa cell microenvironments on endothelial cell status were subsequently evaluated.

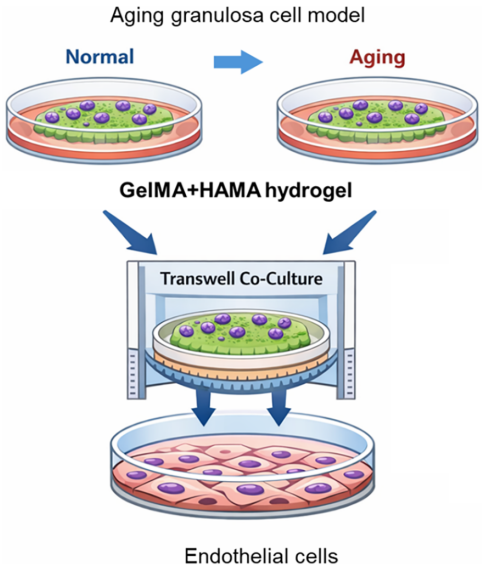

Figure 1. Schematic illustration of the experimental design for the Transwell-based coculture system. Normal and aging granulosa cell models were established in GelMA/HAMA hydrogel and cultured in the upper Transwell insert, while endothelial cells were seeded in the lower chamber. This design allowed soluble factors released from granulosa cells to diffuse across the membrane and influence endothelial cells without direct cell–cell contact

The rheological properties of the hydrogel components and the mixed GH hydrogel are shown in Figure 2. In the frequency sweep test (Figure 2A), both GelMA and HAMA exhibited G′ values higher than G″ throughout the measured frequency range. For both materials, G′ and G″ increased gradually with angular frequency. In addition, the modulus values of GelMA were consistently higher than those of HAMA under the same testing conditions. The gelation behavior of the mixed GH hydrogel was further evaluated by time sweep analysis (Figure 2B). At the initial stage, G″ was higher than G′. With increasing time, G′ rose rapidly and crossed G″, after which G′ remained higher than G″ for the rest of the measurement period. At later time points, both curves tended to level off, with G′ maintaining a markedly higher value than G″. Together, these data indicate that the GH system underwent a time-dependent sol-to-gel transition and formed a hydrogel with predominantly elastic behavior under the tested conditions.

The tensile properties of GelMA and GH hydrogels are shown in Figure 3. Both materials exhibited nonlinear stress–strain behavior, with stress increasing progressively as strain increased. Over the entire strain range, the GH hydrogel displayed higher stress values than GelMA at comparable strain levels. In addition, the GH hydrogel sustained deformation to a higher strain before reaching the end of the curve, whereas the GelMA hydrogel showed a lower maximum strain. These results indicate differences in mechanical response between the two hydrogels under tensile loading.

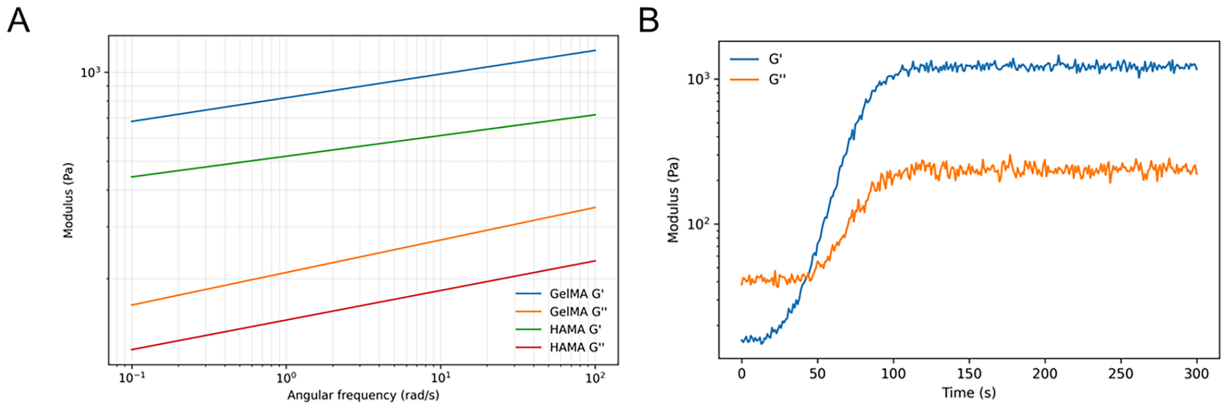

Figure 2. Rheological characterization of GelMA, HAMA, and GH hydrogel. (A) Frequency sweep curves of GelMA and HAMA, showing the storage modulus (G′) and loss modulus (G″) over the tested angular frequency range. (B) Time sweep curve of GH hydrogel during gelation. Changes in G′ and G″ were recorded as a function of time, showing the evolution of viscoelastic behavior during the gelation process

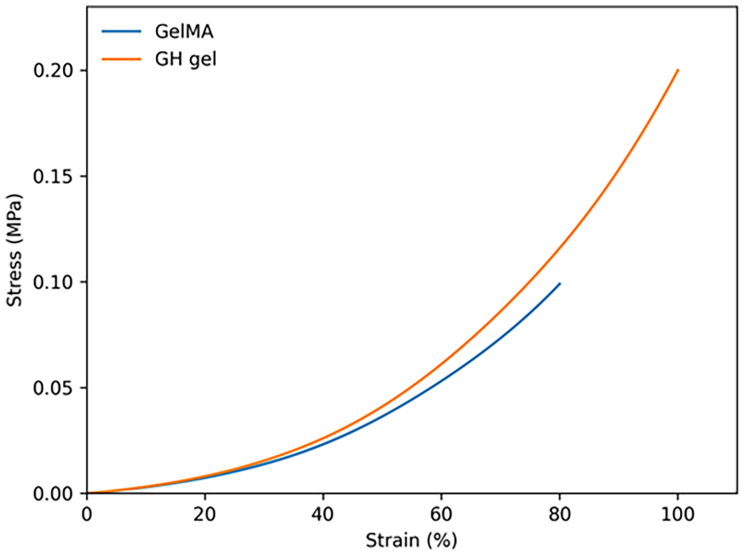

Figure 3. Tensile stress–strain behavior of GelMA and GH hydrogels. Representative stress–strain curves of GelMA and GH hydrogels obtained from uniaxial tensile testing, showing their mechanical response over the measured strain range

Figure 4A shows the internal microstructure of GelMA and GH hydrogels observed by SEM after freeze-drying. Both hydrogels exhibited porous architectures with interconnected pore walls, indicating the formation of continuous three-dimensional networks. Compared with GelMA, the GH hydrogel showed a denser and more compact porous structure, suggesting that the incorporation of HAMA influenced the internal network morphology of the hydrogel. The swelling behavior of the two hydrogels is shown in Figure 4B. Both groups displayed rapid water uptake during the initial incubation period, followed by a gradual approach to equilibrium. However, GelMA maintained a higher swelling ratio than the GH hydrogel throughout most of the tested period and reached a higher equilibrium swelling level. In contrast, the GH hydrogel showed a lower swelling ratio and a more restricted swelling profile,

which may be attributed to the modified network structure after HAMA incorporation. These results indicate that the GH hydrogel formed an interconnected porous matrix while exhibiting more controlled swelling behavior than GelMA under the tested conditions.

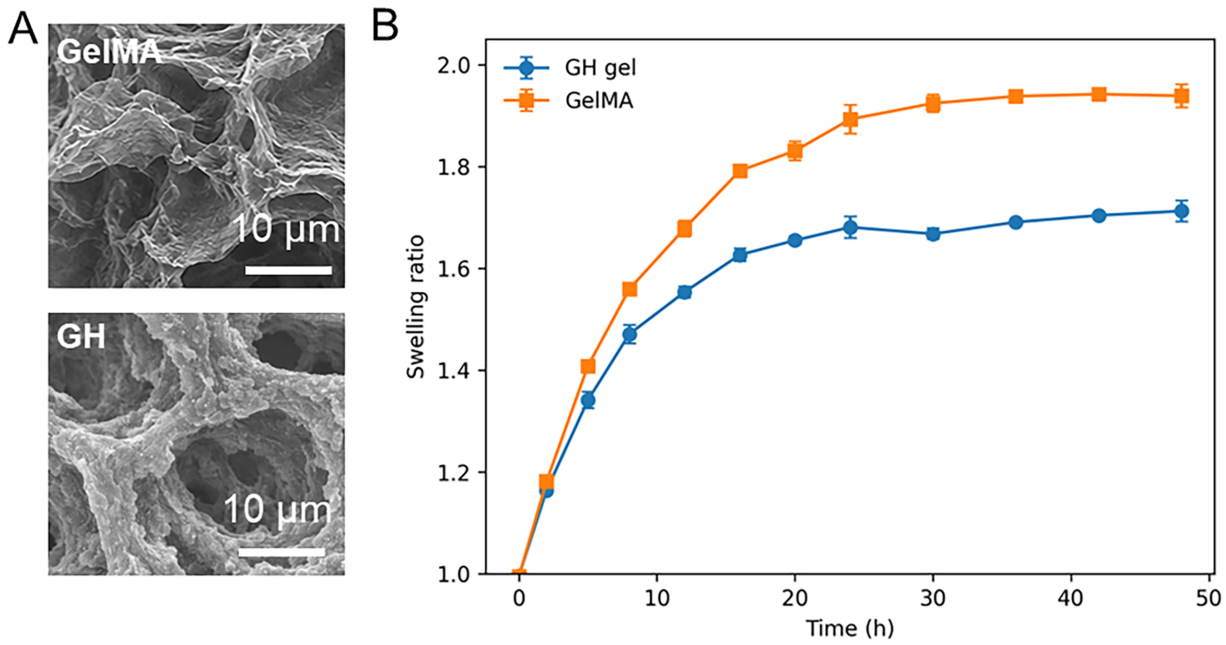

Figure 4. Microstructure and swelling behavior of GH and GelMA hydrogel. (A) Representative SEM image of the GelMA and GH hydrogel, showing its internal porous morphology after freeze-drying. Scale bar: 10 μm. (B) Swelling curves of GH hydrogel and GelMA over the tested time period, showing the time-dependent change in swelling ratio

Figure 5A shows the degradation behavior of GH hydrogel and GelMA under the tested conditions. For both groups, the remaining mass decreased progressively over time, indicating continuous degradation. GelMA exhibited a faster decrease in mass, with a more pronounced reduction throughout the testing period. In contrast, the GH hydrogel retained a higher proportion of its mass at each time point and showed a slower rate of mass loss. By day 7, the remaining mass of GH hydrogel was visibly higher than that of GelMA. Figure 5B presents the cytocompatibility results of GH hydrogel extracts at different concentrations. Compared with the blank group, the 0.1 g/mL group showed a slight decrease in cell viability without a statistically significant difference. In the 0.2 g/mL group, cell viability was lower than that of the blank group and showed a statistically significant difference. In addition, a significant difference was observed between the 0.1 g/mL and 0.2 g/mL groups.

Figure 6 presents a simplified schematic of the Transwell-based coculture configuration used in this study. Granulosa cells were encapsulated within the GH hydrogel and placed in the upper insert to form the ovarian-side model. Endothelial cells were cultured on the bottom surface of the lower chamber. The Transwell membrane physically separated the two cell populations while permitting the exchange of soluble molecules across compartments. This setup was used to expose endothelial cells to factors released from granulosa cells under defined conditions.

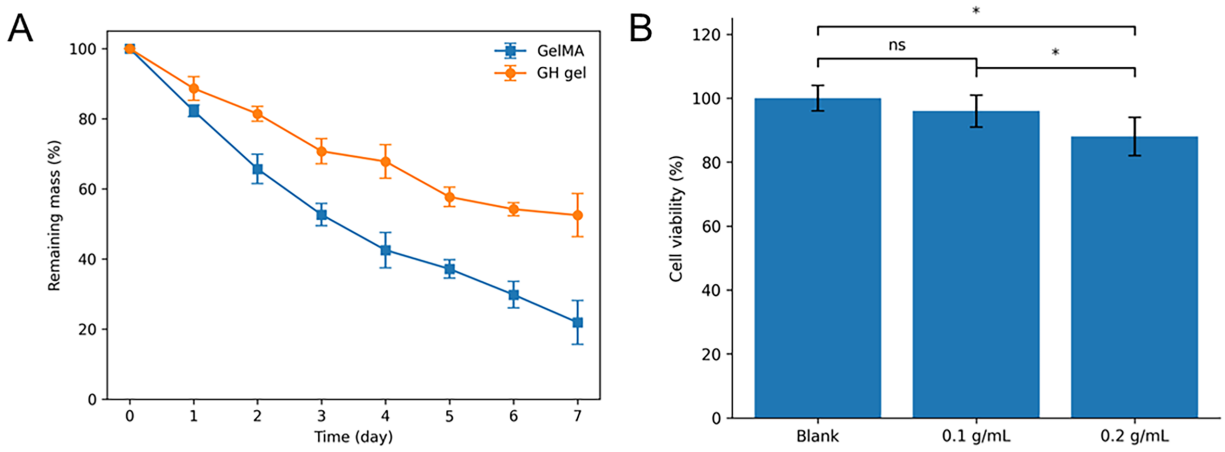

Figure 5. Degradation behavior and cytocompatibility of GH hydrogel. (A) Enzymatic degradation profiles of GH hydrogel and GelMA over 7 days, expressed as remaining mass percentage. (B) Cell viability of cells cultured with different concentrations of GH hydrogel extracts, evaluated by CCK-8 assay. Data are presented as mean ± SD. Statistical significance is indicated as follows: ns, not significant; *$p < 0.05$

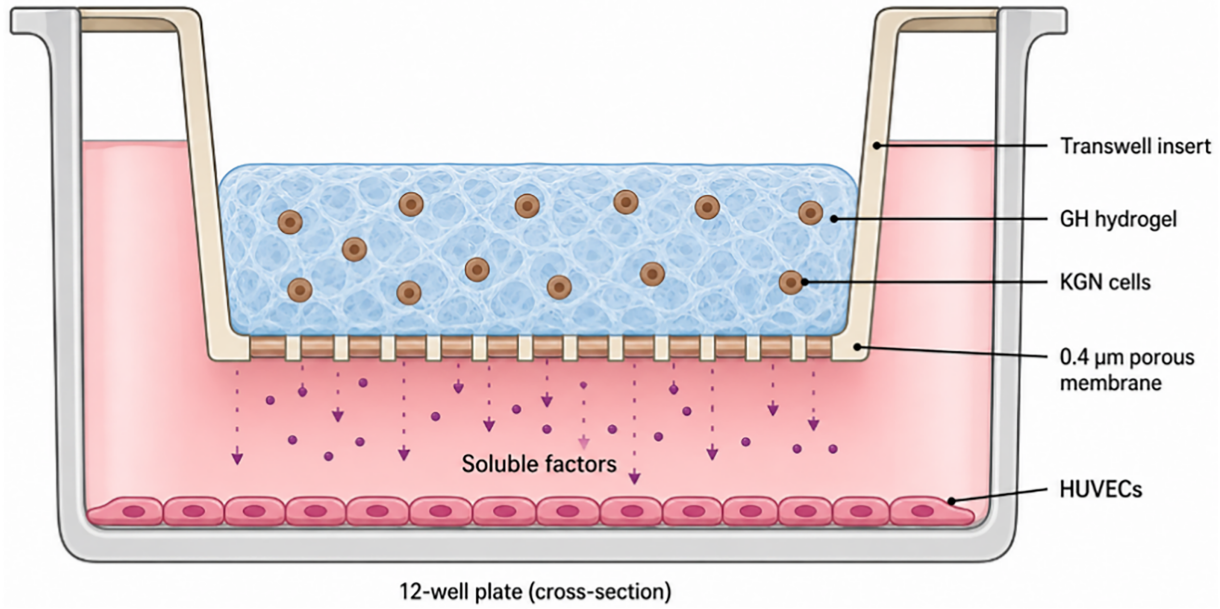

Figure 6. Schematic illustration of the Transwell-based coculture configuration. Granulosa cells embedded in GH hydrogel were cultured in the upper Transwell insert, while endothelial cells were seeded in the lower chamber. The system allows diffusion of soluble factors between the two compartments without direct cell–cell contact

Figure 7 shows the characterization of granulosa cells cultured in GH hydrogel under control and aging conditions. Compared with the control group, the aging model group exhibited a higher ROS level. At the same time, E2 secretion was lower in the aging group than in the control group. In addition, the expression of StAR was reduced in the aging group, whereas the expression of p16 was increased. Statistical analysis indicated significant differences between the two groups for all measured

parameters. These results indicate that the aging-treated granulosa cells displayed changes in oxidative stress, hormone-related function, and senescence-associated markers under the tested conditions.

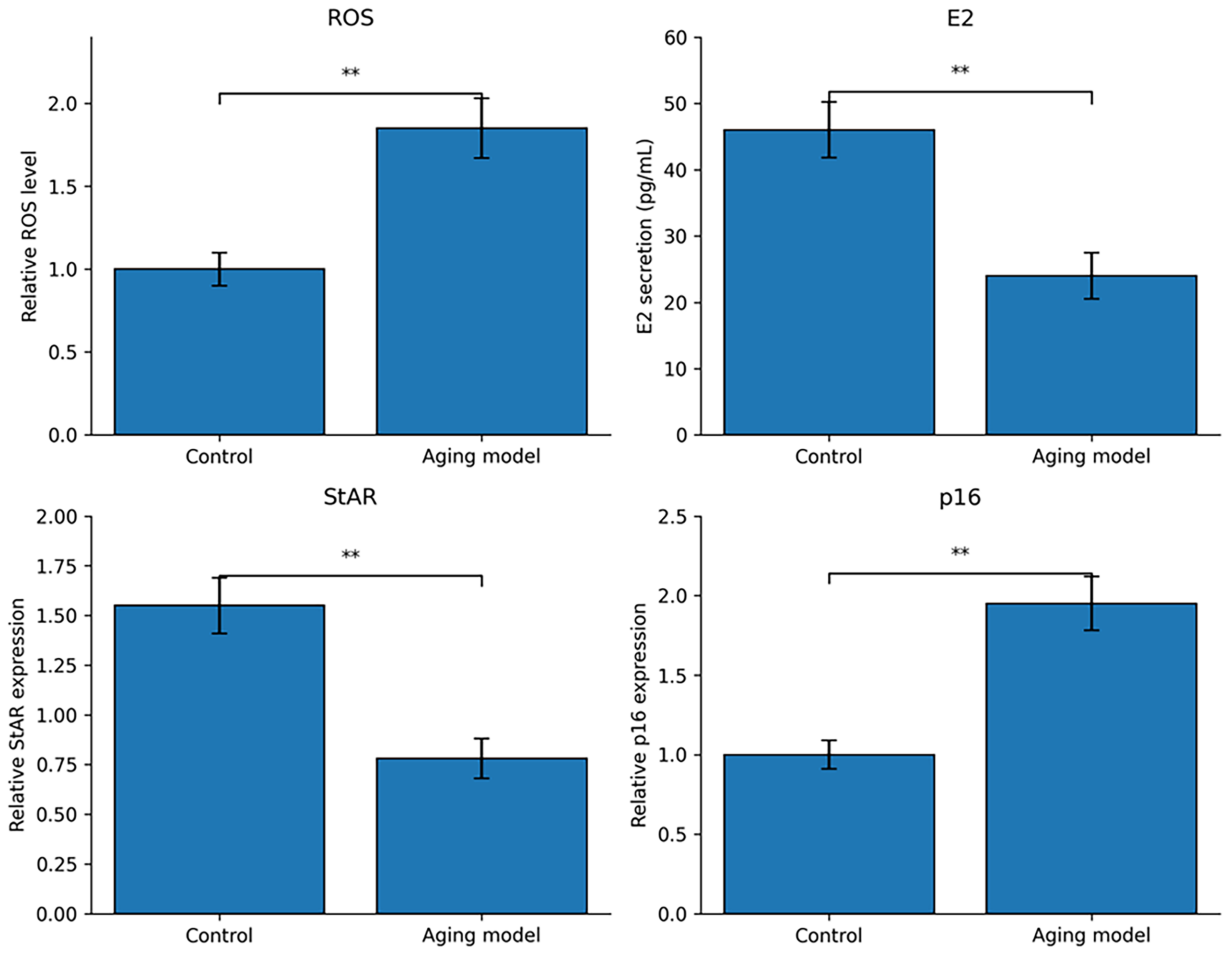

Figure 7. Characterization of the granulosa cell aging model in GH hydrogel. Relative ROS level, E2 secretion, StAR expression, and p16 expression were measured to evaluate oxidative stress, steroidogenic function, and senescence status in granulosa cells cultured in GH hydrogel under control and aging conditions. Data are presented as mean ± SD. Statistical significance is indicated as follows: $^{**}p < 0.01$

Figure 8 shows the response of endothelial cells after exposure to different conditioned media. Compared with the HUVEC control group, treatment with Normal CM resulted in a slight increase in ROS level and VCAM-1 expression, while cell viability showed a small decrease. In the Aging CM group, ROS levels were higher than those in both the control and Normal CM groups. Similarly, VCAM-1 expression increased further in the Aging CM group compared with the other groups. In terms of cell viability, a decreasing trend was observed from the control group to the Normal CM group and further to the Aging CM group. Statistical analysis indicated a significant difference between the control group and the Aging CM group for all three indicators.

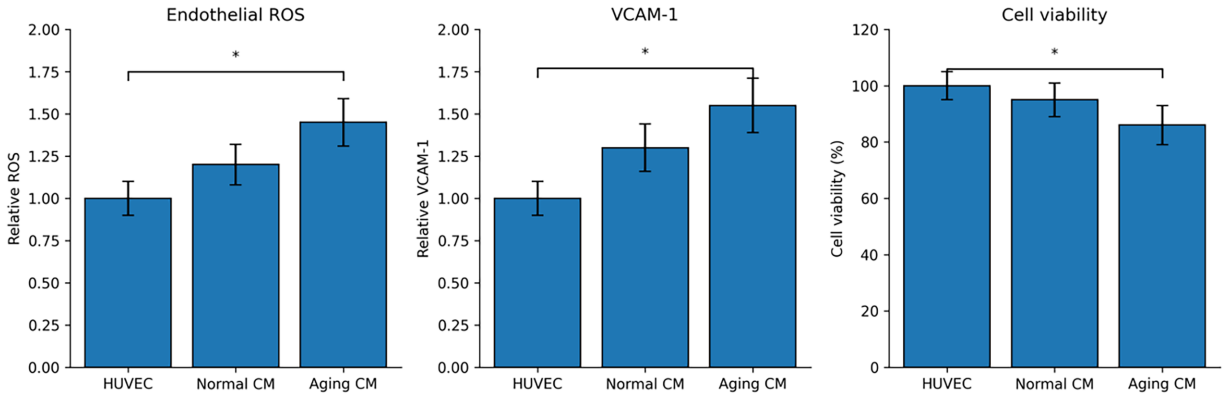

Figure 8. Effects of conditioned media from granulosa cells on endothelial cell status. Relative ROS level, VCAM-1 expression, and cell viability of endothelial cells after treatment with control medium, normal granulosa cell-conditioned medium (Normal CM), and aging granulosa cell-conditioned medium (Aging CM). Data are presented as mean ± SD. Statistical significance is indicated as follows: ns, not significant; *$p < 0.05$

4. Discussion

The Transwell-based design shown in Figure 1 was intended to provide a simplified platform for studying the interaction between granulosa cells and endothelial cells [14]. In this system, GelMA/HAMA hydrogel served as a three-dimensional matrix for granulosa cell culture in the upper compartment, whereas endothelial cells were maintained separately in the lower chamber. This arrangement reduced direct physical interference between the two cell populations and made it possible to focus on diffusion-mediated paracrine effects. It should be noted that this model does not reproduce the full structural complexity of ovarian or vascular tissues. Instead, it provides a controllable *in vitro* setting for examining whether changes in granulosa cell state are accompanied by corresponding changes in endothelial cell behavior. Therefore, the significance of this design lies primarily in establishing an experimental framework for cell–cell interaction analysis rather than fully recapitulating the *in vivo* microenvironment [15,16]. The main contribution of this model is the combination of three components: a GelMA/HAMA hydrogel matrix for three-dimensional granulosa cell encapsulation, an H_2O_2-induced aging-like granulosa cell state, and a Transwell-based endothelial response compartment. Therefore, the platform differs from previous hydrogel-only or coculture-only systems by linking a defined hydrogel-supported granulosa cell model with downstream endothelial cell responses. This arrangement allows the effect of soluble factors released from aging-like granulosa cells to be evaluated under controlled *in vitro* conditions.

Figure 2 provides rheological evidence for the viscoelastic characteristics of the precursor components and the gelation process of the mixed system. The observation that G′ remained higher than G″ for both GelMA and HAMA in the frequency sweep test suggests that both materials displayed solid-like behavior within the tested range. The higher modulus of GelMA relative to HAMA indicates that the two components contributed differently to the overall mechanical response of the system. In the GH time sweep curve, the crossover of G′ and G″ followed by sustained dominance of G′ is consistent with gel formation during the measurement period. This result supports the use of the mixed system as a stable hydrogel matrix in subsequent cell culture experiments. These rheological results support the formation of a stable hydrogel matrix suitable for subsequent cell culture experiments. The rheological results here should be interpreted as evidence of gelation behavior and relative viscoelastic properties rather than as a complete assessment of hydrogel function [17].

The stress–strain curves in Figure 3 suggest that the GH hydrogel exhibited higher stress at similar strain levels and a greater deformation range compared to GelMA under the tested conditions. This difference may be related to the combined contribution of GelMA and HAMA in the mixed system, which could influence the mechanical response during stretching. The data here support a difference in tensile behavior between the two hydrogels but should be interpreted within the limits of the measured stress–strain relationship [18].

The data in Figure 4 provide basic structural and hydration-related information for the GH hydrogel. The porous morphology observed by SEM suggests that the hydrogel possessed an open internal network rather than a compact bulk structure, which is a common feature of freeze-dried hydrated polymer systems. At the same time, the swelling experiment showed that both GH hydrogel and GelMA were able to absorb water rapidly at the beginning of incubation and then gradually reached a stable state, indicating typical time-dependent swelling behavior [19]. The lower swelling ratio of GH hydrogel relative to GelMA suggests that the incorporation of HAMA changed the hydration behavior of the mixed system under the tested conditions. This difference may reflect changes in network composition or the balance between water uptake and structural restriction, this difference may be related to changes in network composition and water-retention behavior after HAMA incorporation [20]. Based on Figure 4 alone, it is more appropriate to conclude that GH hydrogel exhibited a porous structure and a lower equilibrium swelling ratio than GelMA, rather than to make broader claims regarding its network architecture or biological consequences.

The results in Figure 5 indicate that the GH hydrogel and GelMA exhibited different degradation behaviors under the tested conditions. The slower mass loss observed for the GH hydrogel suggests that the introduction of HAMA influenced the degradation profile of the system. However, the data presented here are limited to overall mass change and do not provide information on degradation mechanisms or intermediate structural changes [21]. The cytocompatibility results further show that GH hydrogel extracts did not lead to a marked reduction in cell viability at lower concentration (0.1 g/mL), while a moderate decrease was observed at higher concentration (0.2 g/mL). These findings suggest that the hydrogel extract exhibited concentration-dependent effects on cell viability under the tested conditions [22]. The data support that GH hydrogel shows a relatively slower degradation profile compared with GelMA and maintains acceptable cell compatibility within the evaluated concentration range, although further studies would be required to assess long-term biological responses.

The configuration shown in Figure 6 provides a controlled *in vitro* system for examining interactions between granulosa cells and endothelial cells through soluble factor exchange. By spatially separating the two cell types, the model reduces direct contact effects and focuses on paracrine signaling [23]. At the same time, the use of GH hydrogel in the upper compartment provides a three-dimensional environment for granulosa cells, which differs from conventional two-dimensional culture. However, this system does not replicate the full structural or biochemical complexity of native ovarian or vascular tissues [24]. Therefore, the observations derived from this model should be interpreted as evidence of interaction under simplified conditions rather than a complete representation of *in vivo* processes [25].

The data in Figure 7 provide a set of indicators describing the state of granulosa cells in the GH hydrogel system under aging-related treatment. The increase in ROS suggests the presence of oxidative stress, while the decrease in E2 secretion and StAR expression reflects changes in steroidogenic activity. It should be noted that the increase in ROS observed in this study was mainly associated with H_2O_2 treatment rather than with the GH hydrogel itself. In this system, the GH hydrogel served as a three-dimensional matrix for KGN cell encapsulation and culture, while H_2O_2 was used as the oxidative stimulus to induce an aging-like cellular state. Therefore, the elevated ROS level reflects the oxidative stress response of KGN cells within the hydrogel environment. Together with increased p16 expression and reduced E2 secretion and StAR expression, this result supports the successful establishment of an aging-like granulosa cell model in the GH hydrogel. The elevated p16 expression indicates an increase in senescence-associated characteristics [26]. Taken together, these observations support that the applied

treatment induced measurable changes in granulosa cell status within the hydrogel environment. These results are limited to the selected markers and experimental conditions, and do not fully capture the complexity of ovarian aging *in vivo* [27,28]. Therefore, the findings here should be interpreted as evidence of an *in vitro* aging-like state rather than a direct representation of physiological aging processes [29].

The data in Figure 8 show that conditioned media derived from granulosa cells under different states were associated with measurable changes in endothelial cell behavior. The increase in ROS and VCAM-1 expression in the Aging CM group suggests that factors present in this conditioned medium were associated with elevated oxidative stress and inflammatory marker expression in endothelial cells [30]. At the same time, the observed reduction in cell viability indicates a change in cell status under these conditions [31]. Compared with Aging CM, the effects of Normal CM on endothelial cells were relatively modest, indicating that the state of granulosa cells may influence the composition of released factors. However, the present data do not identify specific mediators responsible for these effects, and the observed changes are limited to the selected endpoints. Therefore, the results support an association between granulosa cell state and endothelial cell response under the tested conditions, but do not establish a direct causal mechanism [32].

5. Conclusion

In this study, a GH hydrogel-based *in vitro* platform was established to support granulosa cell culture and to investigate granulosa cell–endothelial cell interaction under Transwell conditions. Rheological analysis showed that the mixed system underwent gelation and exhibited stable viscoelastic behavior, while the tensile, swelling, and degradation results further indicated that GH hydrogel displayed material properties distinct from those of GelMA alone. The hydrogel also showed acceptable cytocompatibility within the tested concentration range, supporting its use as a cell culture matrix. Using this platform, an aging-like granulosa cell model was generated in GH hydrogel. Compared with the control group, the aging model showed increased ROS and p16 expression, together with reduced E2 secretion and StAR expression, indicating that the treated granulosa cells underwent measurable changes in oxidative stress, senescence-associated status, and steroidogenic function under the present experimental conditions. Conditioned medium experiments further showed that endothelial cells exposed to medium derived from the aging granulosa cell model exhibited higher ROS and VCAM-1 levels and lower cell viability than the control group, while the changes induced by normal conditioned medium were relatively limited. These results suggest that the state of granulosa cells may influence endothelial cell responses through soluble factors. Overall, this work provides a controllable *in vitro* model for studying the interaction between granulosa cell aging-like changes and endothelial cell status, although the specific mediators and mechanisms involved require further investigation.

Acknowledgement: Not applicable.

Funding Statement: The study was supported by the Top Talent Support Program for young and middle-aged people of Wuxi Health Committee (Grant No. BJ2023076).

Author Contributions: Qianqian Ma was responsible for conceptualization, writing the original draft, reviewing and editing the manuscript, and supervision. Han Zheng and Ailing Chen contributed to data curation, funding acquisition, investigation, and drafting the original manuscript. Jingfen Cai was involved in resources, software, and validation. Lifeng Zhang and Yanfang Gu took charge of supervision, project administration, and formal analysis. All authors reviewed and approved the final version of the manuscript.

Availability of Data and Materials: The datasets generated and/or analyzed during the current study are available from the corresponding authors upon reasonable request.

Ethics Approval: Not applicable.

Conflicts of Interest: The authors declare no conflicts of interest.

Abbreviations

GH	GelMA/HAMA
GelMA	Gelatin methacrylate
HAMA	Methacrylated hyaluronic acid
LAP	Lithium phenyl-2,4,6-trimethylbenzoylphosphinate
DMEM/F12	Dulbecco's modified Eagle's medium/Ham's F-12
FBS	Fetal bovine serum
PBS	Phosphate-buffered saline
H_2O_2	Hydrogen peroxide
DCFH-DA	Dichlorodihydrofluorescein diacetate
HUVECs	Human umbilical vein endothelial cells
SD	Standard deviation

References

1. Berg ICE. Investigating the role of geometry, mechanics, and microenvironmental cues on liver progenitor cell differentiation [dissertation]. Champaign, IL, USA: University of Illinois at Urbana-Champaign; 2021.
2. Hosokawa M, Ueno M. Aging of blood-brain barrier and neuronal cells of eye and ear in SAM mice. Neurobiol Aging. 1999;20(2):117–23. doi:10.1016/s0197-4580(99)00029-9.
3. Caretti M, Potenza DM, Ajalbert G, Albrecht U, Ming XF, Brenna A, et al. Arginase-II gene deficiency reduces skeletal muscle aging in mice. Aging. 2024;16(22):13563–87. doi:10.18632/aging.206173.
4. Dhawan A, Friedrichs J, Bray L, Hofbauer LC, Wobus M, Bornhäuser M. Interaction of tumor cells with the hematopoietic stem and progenitor cell niche. Blood. 2014;124(21):5139. doi:10.1182/blood.v124.21.5139.5139.
5. Chung KW, Ha S, Kim SM, Kim DH, An HJ, Lee EK, et al. PPARα/β activation alleviates age-associated renal fibrosis in sprague dawley rats. J Gerontol Ser A. 2020;75:452–8. doi:10.1093/gerona/glz083.
6. Bracken SJ, Poe JC, Sarantopoulos S. What's atypical about human B cells after allogeneic stem cell transplantation? J Leukoc Biol. 2025;117(5):qiaf048. doi:10.1093/jleuko/qiaf048.
7. Mihajlovic M, Pásztor-Jánoska DK, Cadenas J, Adrados CS, Andersen CY, Kristensen SG, et al. 3D culture of ovarian follicles in granular and nanofibrillar hydrogels. Biomater Adv. 2024;164(1):213987. doi:10.1016/j.bioadv.2024.213987.
8. Gao Q, Liu Z, Lin Z, Qiu J, Liu Y, Liu A, et al. 3D bioprinting of vessel-like structures with multilevel fluidic channels. ACS Biomater Sci Eng. 2017;3(3):399–408. doi:10.1021/acsbiomaterials.6b00643.
9. Yang D, Sun B, Li S, Wei W, Liu X, Cui X, et al. NKG2D-CAR T cells eliminate senescent cells in aged mice and nonhuman Primates. Sci Transl Med. 2023;15(709):eadd1951. doi:10.1126/scitranslmed.add1951.
10. Hashimoto M, Asai A, Kawagishi H, Mikawa R, Iwashita Y, Kanayama K, et al. Elimination of $p19^{ARF}$-expressing cells enhances pulmonary function in mice. JCI Insight. 2016;1(12):e87732. doi:10.1172/jci.insight.87732.
11. Han S, Kim J, Kim SH, Youn W, Kim J, Ji GY, et al. *In vitro* induction of *in vivo*-relevant stellate astrocytes in 3D brain-derived, decellularized extracellular matrices. Acta Biomater. 2023;172:218–33. doi:10.1016/j.actbio.2023.09.046.

12. He M, Chiang HH, Luo H, Zheng Z, Qiao Q, Wang L, et al. An acetylation switch of the NLRP3 inflammasome regulates aging-associated chronic inflammation and insulin resistance. Cell Metab. 2020;31(3):580–91.e5. doi:10.1016/j.cmet.2020.01.009.
13. Itami N, Kawahara-Miki R, Kawana H, Endo M, Kuwayama T, Iwata H. Age-associated changes in bovine oocytes and granulosa cell complexes collected from early antral follicles. J Assist Reprod Genet. 2014;31(8):1079–88. doi:10.1007/s10815-014-0251-y.
14. Ito M, Imai M, Muraki M, Miyado K, Qin J, Kyuwa S, et al. GSTT1 is upregulated by oxidative stress through p38-mk2 signaling pathway in human granulosa cells: possible association with mitochondrial activity. Aging. 2011;3(12):1213–23. doi: 10.18632/aging.100418.
15. Iwata H. Age-associated changes in granulosa cells and follicular fluid in cows. J Reprod Dev. 2017;63(4):339–45. doi:10.1262/jrd.2017-048.
16. Jeong Y, Han X, Vyas K, Irudayaraj J. Microbial β-glucuronidase hydrogel beads activate chemotherapeutic prodrug. ACS Appl Mater Interfaces. 2024;16(22):28093–103. doi:10.1021/acsami.4c02568.
17. Jeong Y, Hsieh PH, Phal Y, Bhargava R, Irudayaraj J. Label-free monitoring of coculture system dynamics: probing probiotic and cancer cell interactions via infrared spectroscopic imaging. Anal Chem. 2024;96(28):11247–54. doi:10.1021/acs.analchem.4c00894.
18. Jiao D, Xie L, Xing W. A pumpless liver-on-a-chip for drug hepatotoxicity analysis. Analyst. 2024;149(18):4675–86. doi:10.1039/d4an00602j.
19. Saeed GA, Farooq N. Precocious pseudopuberty due to juvenile granulosa cell tumor. J Coll Physicians Surg Pak. 2003;13(6):287–8. doi:10.1016/s0022-3468(67)80053-8.
20. Sedivy JM, Banumathy G, Adams PD. Aging by epigenetics—a consequence of chromatin damage? Exp Cell Res. 2008;314(9):1909–17. doi:10.1016/j.yexcr.2008.02.023.
21. Pan WJ, Shi LL, Ren YR, Yao CY, Lu YM, Chen Y. Polysaccharide ORP-1 isolated from *Oudemansiella raphanipes* ameliorates age-associated intestinal epithelial barrier dysfunction in Caco-2 cells monolayer. Food Res Int. 2022;162(Pt A):112038. doi:10.1016/j.foodres.2022.112038.
22. Pajoumshariati SR, Azizi M, Zhang S, Dogan B, Simpson KW, Abbaspourrad A. A microfluidic-based model for spatially constrained culture of intestinal microbiota. Adv Funct Mater. 2018;28(48):1805568. doi:10.1002/adfm.201805568.
23. Sun N, Cheng X, Lu L, Zhang W, Li K, Chen Y, et al. Nicotinamide riboside improves mitochondrial function and oocyte maturation in aged mice: a multitarget mechanistic study using network pharmacology and molecular simulations. J Food Biochem. 2026;2026(1):2506427. doi:10.1155/jfbc/2506427.
24. Matzkin H, Braf Z, Nava D. Does age influence the bioactivity of follicle-stimulating hormone in men? Age Ageing. 1991;20(3):199–205. doi:10.1093/ageing/20.3.199.
25. Wang K, Wu D, Zhang H, Das A, Basu M, Malin J, et al. Comprehensive map of age-associated splicing changes across human tissues and their contributions to age-associated diseases. Sci Rep. 2018;8(1):10929. doi:10.1038/s41598-018-29086-2.
26. Liu Y, Rayatpisheh S, Chew SY, Chan-Park MB. Impact of endothelial cells on 3D cultured smooth muscle cells in a biomimetic hydrogel. ACS Appl Mater Interfaces. 2012;4(3):1378–87. doi:10.1021/am201648f.
27. Korsakova NV, Sergeeva VE, Petrov SB. Immunohistochemical analysis of the lens cells during development of the various types of age-associated cataract in man. Morfologiia Saint Petersburg Russ. 2007;132(5):47–51. doi:10.1007/s11055-008-9066-6.
28. Lu B, Christensen I, Ma L, Wang X, Jiang L, Wang C, et al. miR-24-p53 pathway evoked by oxidative stress promotes lens epithelial cell apoptosis in age-related cataracts. Mol Med Report. 2018;17(4):5021–8. doi:10.3892/mmr.2018.8492.

29. Wang S, Zheng Y, Li J, Yu Y, Zhang W, Song M, et al. Single-cell transcriptomic atlas of primate ovarian aging. Cell. 2020;180(3):585–600. doi:10.1016/j.cell.2020.01.009.
30. Ma J, Chen S, Liu J, Liao Y, Li L, Wang CC, et al. Cryptochrome 1 regulates ovarian granulosa cell senescence through NCOA4-mediated ferritinophagy. Free Radic Biol Med. 2024;217:1–14. doi:10.1016/j.freeradbiomed.2024.03.015.
31. Xu L, Idrees M, Joo MD, Sidrat T, Wei Y, Song SH, et al. Constitutive expression of TERT enhances β-Klotho expression and improves age-related deterioration in early bovine embryos. Int J Mol Sci. 2021;22(10):5327. doi:10.3390/ijms22105327.
32. Kong Y, Trabucco SE, Zhang H. Oxidative stress, mitochondrial dysfunction and the mitochondria theory of aging. In: Robert L, Fulop T, editors. Aging: facts and theories. Basel, Switzerland: Karger; 2014. p. 86–107. doi:10.1159/000358901.

Received: 09 April 2026; Accepted: 11 June 2026; Published: xx xx 2026